Influence of the SEI Formation on the Stability and Lithium Diffusion in Si Electrodes

ACS OMEGA

http://pubs.acs.org/journal/acsodf

Article

Influence of the SEI Formation on the Stability and Lithium Diffusion in Si Electrodes

Baolin Wu, Chunguang Chen,* Dmitri L. Danilov, Ming Jiang, Luc H. J. Raijmakers, Rüdiger-A. Eichel, and Peter H. L. Notten*

Cite This: *ACS Omega* 2022, 7, 32740−32748

Read Online

ACCESS | Metrics & More | Article Recommendations | Supporting Information

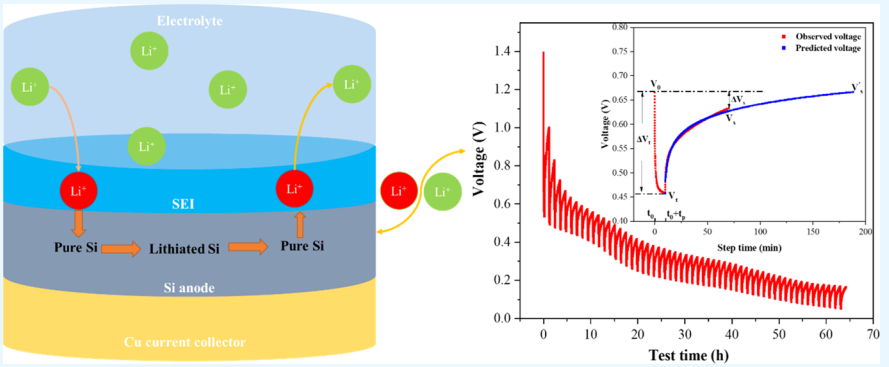

ABSTRACT: Silicon (Si) is an attractive anode material for Li-ion batteries (LIBs) due to its high theoretical specific capacity. However, the solid−electrolyte interphase (SEI) formation, caused by liquid electrolyte decomposition, often befalls Si electrodes. The SEI layer is less Li-ion conductive, which would significantly inhibit Li-ion transport and delay the reaction kinetics. Understanding the interaction between the SEI components and Li-ion diffusion is crucial for further improving the cycling performance of Si. Herein, different liquid electrolytes are applied to investigate the induced SEI components, structures, and their role in Li-ion transport. It is found that Si electrodes exhibit higher discharge capacities in $LiClO_4$-based electrolytes than in $LiPF_6$-based electrolytes. This behavior suggests that a denser and more conductive SEI layer is formed in $LiClO_4$-based electrolytes. In addition, a coating of a Li_3PO_4 artificial SEI layer on Si suppresses the formation of natural SEI formation, leading to higher capacity retentions. Furthermore, galvanostatic intermittent titration technique (GITT) measurements are applied to calculate Li-ion diffusion coefficients, which are found in the range of 10^{-23}−10^{-19} m^2/s.

1. INTRODUCTION

Lithium-ion battery (LIB) technology has become the most popular battery type in electric vehicles, communication devices, and portable electronics due to its superior properties, e.g., higher energy density, higher voltage, and lower self-discharge than other energy-storage systems.[1−4] With the demands of life, many requirements of high energy and power densities in such applications intensified the search for stable and robust Li-ion intercalation capacity compounds as active Li host materials in Li-ion battery electrodes.[5] In recent years, various high-capacity anode materials have been explored. Si is deemed one of the most promising anode materials for next-generation LIBs with the high specific capacity of 3579 mAh/g, low reaction potential of 0.4 V vs Li/Li^+, low cost, natural abundance, environmental friendliness, and safety.[6−8]

Nowadays, some drawbacks still hinder the commercial breakthrough of Si electrodes, e.g., solid−electrolyte interphase (SEI) formation, low intrinsic electronic/Li-ionic conductivity, and severe volume changes (up to 300%).[9,10] The SEI is a significant drawback for the Si anode. SEI is a multiple-layered film formed at the interface between Si and the electrolyte due to electrolyte decomposition.[11] The SEI layer formed on the Si surface will affect the electrochemical performance of Si anodes. For example, SEI will decrease the capacity retention rate of Si. Due to the irreversible formation of SEI, about 15% of the total charge is lost upon lithiation.[12] In addition, the formed SEI layer will hinder the insertion/extraction of Li-ions, delaying the electrochemical reaction kinetics. Many studies revealed that the SEI on Si has a double-layer structure composed of an inner and an outer layer.[13−15] The inner SEI is predominantly composed of inorganic substances, including LiF, Li_2O, and Li_2CO_3, which

Received: July 13, 2022
Accepted: August 16, 2022
Published: August 30, 2022

are dense, thin, and relatively stable.[16,17] The outer SEI layer is located on the top of the inner SEI layer. It is primarily made up of organic materials, such as $ROCO_2Li$ (where R is a low-molecular-weight alkyl group), and continues to grow during cycling.[18−20] Chen et al. further suggested that the inner SEI layer is 1.5 times less Li-ionic conductive than the outer SEI. Thus, the transport of Li-ions through the inner SEI plays a critical limiting role in Si electrodes.

In recent years, the fast charging/discharging capability (>6 C) of electrode materials has been a critical performance requirement of LIB for future electric vehicle applications. The Li-ion diffusion coefficient largely defines the fast charging/discharging properties of an electrode. Therefore, studying the Li-ion diffusion coefficient of Si thin-film anodes is very important for its application. The chemical diffusivity in Si electrodes is also investigated by various electrochemical methods, such as cyclic voltammetry (CV),[21−23] electrochemical impedance spectroscopy (EIS),[24,25] and potentiostatic intermittent titration (PITT)[26−28] or galvanostatic intermittent titration (GITT).[29−31] In GITT, a cell is exposed to a series of continuous current pulses, alternately between relatively short discharge/charge steps and relatively long rest steps, to determine critical physical characteristics, including the reaction rate constant, open-circuit voltage (OCV), and diffusion coefficient.[32] However, most of the relaxation times used in the literature to determine the Li-ion diffusion coefficient of the Si anode by GITT are very short (less than 20 min).[29,33] Si anodes cannot reach the equilibrium state under such short relaxation times due to chemical reaction, which reduces the accuracy of the measured values.

In this work, we first compare the electrochemical performances of 50 nm Si thin-film anodes with $LiClO_4$-based and $LiPF_6$-based electrolytes and found that the Si anode is more stable in $LiClO_4$-based electrolytes. The thickness, morphology, and composition of the formed SEI layers are systematically studied, which are the main factors to affect the stability. The morphology of the SEI layer formed in $LiClO_4$-based electrolytes was found to be denser and smoother, which improves the stability. Moreover, the formed SEI layers were measured by time-of-flight secondary ion mass spectrometry (ToF-SIMS) to analyze the compositions across the thickness. In addition, we also deposited a Li_3PO_4 layer on the Si surface, which confirmed that the Li_3PO_4 layer could suppress the SEI layer formation. It was found that Li_3PO_4 can improve the Coulombic efficiency and stability of Si anodes, indicating that Li_3PO_4 is an excellent artificial layer to protect Si anodes. Finally, GITT measurements were carried out on these samples, and the relaxation time was extended to 3 h by the so-called voltage-prediction method so that the electrode could be considered to reach the equilibrium state.[34] The corresponding Li-ion diffusion coefficients during the discharge process calculated by GITT measurements are found to be more accurate.

2. EXPERIMENTAL SECTION

2.1. Synthesis. All sputter deposition targets (Cu, Si, and Li_3PO_4) were obtained from Advanced Engineering Materials Co., China. Si wafers with 4 in. diameters were used as substrates. A physical vapor deposition (PVD) system (Kurt J. Lesker, U.K.) was used to prepare samples. A Cu layer, 150 nm thick, was deposited onto the Si crystalline substrates by thermal evaporation. Then, an amorphous 50 nm thick Si film was deposited on Cu by direct-current magnetron sputtering as thin-film electrodes. Furthermore, the artificial layer of 60 nm Li_3PO_4 thin films was deposited by RF magnetron sputtering (Figure S1). A chamber pressure of 5 mTorr and a sputtering power of 90 W in an Ar atmosphere were used in the sputtering process.

2.2. Characterization. Scanning electron microscopy (SEM) images were taken on by a Quanta FEG 650 (FEI) environmental scanning electron microscope operated at a voltage of 20 kV. Time-of-flight secondary ion mass spectrometry (ToF-SIMS) analyses were performed by the ToF-SIMS IV of the company ION-TOF (Münster, Germany), and depth profiling was carried out by a 30 keV ion source beam.

2.3. Electrochemical Measurements. The electrochemical performance of Si electrodes was tested in custom-made Teflon cells, of which the schematic layout can be found elsewhere.[35] The surface area of Si electrodes is well-defined with 1.54 cm^2 for the electrochemical test. Two Li-metal electrodes were used as the counter and reference electrodes. 1 M $LiClO_4$ and 1 M $LiPF_6$ dissolved in propylene carbonate (PC) and 1 M $LiPF_6$ in ethylene carbonate (EC)/dimethyl carbonate (DMC)/diethyl carbonate (DEC) (1:1:1 in a volume ratio) were used as liquid electrolytes. All electrochemical measurements were performed in an Ar-filled glovebox with an M2300 galvanostat (Maccor). Galvanostatic charge/discharge cycling was performed in the voltage range of 0.05−1.5 V vs Li/Li^+. Galvanostatic intermittent titration (GITT) measurements were carried out with a small current of 0.15 C. Each pulse lasted 10 min and was followed by a 60 min resting period in the GITT tests.[36] All GITT measurements were carried out at room temperature.

2.4. Voltage-Relaxation Model. In this work, a voltage-prediction method was applied to analyze the GITT data. Instead, the voltage-relaxation end value is determined from the measured first part of a voltage-relaxation curve and mathematical optimization/fitting function.[35,36] Furthermore, the function contains three more parameters that are also determined by fitting. This property implies that these parameters are updated for each situation. The following derived expression describes the general model for the voltage-relaxation process used in the GITT analyses[37]

$$V_t = a_0 - \frac{a_3}{t^{a_1}[\log(t)]^{a_2}} e^{\varepsilon_t/2} \tag{1}$$

where $a_1 > 0$, $a_2 > 0$, and $a_3 > 0$ are rate-determining constants and a_0 is the final relaxation voltage (an asymptotical value, i.e., EMF), V_t is the relaxation voltage at time t, $[\log(t)]^{a_2}$ is the natural logarithm (with base e) of time [s] in the power a_2, and ε is a random error term.

The parameters a_i for i from 0 to 3 can be estimated by applying the (concentrated) ordinary least-squares (OLS) scheme. For that, eq 1 can be rearranged by taking squared values

$$\left(\frac{a_3}{t^{a_1}[\log(t)]^{a_2}}\right)^2 = (a_0 - V_t)^2 e^{-\varepsilon_t} \tag{2}$$

Taking the natural logarithm of both sides reduces eq 2 to a usual linear regression model

$$\log([a_0 - V_t]^2) = A_1 + A_2\log(t) + A_3\log(\log(t)) + \varepsilon_t \tag{3}$$

where $A_1 = 2\log(a_3)$, $A_2 = -2a_1$, and $A_3 = -2a_2$. For each fixed value of a_0, eq 3 can be written as the usual regression model

$$y = X\alpha + \varepsilon \tag{4}$$

https://doi.org/10.1021/acsomega.2c04415
ACS Omega 2022, 7, 32740−32748

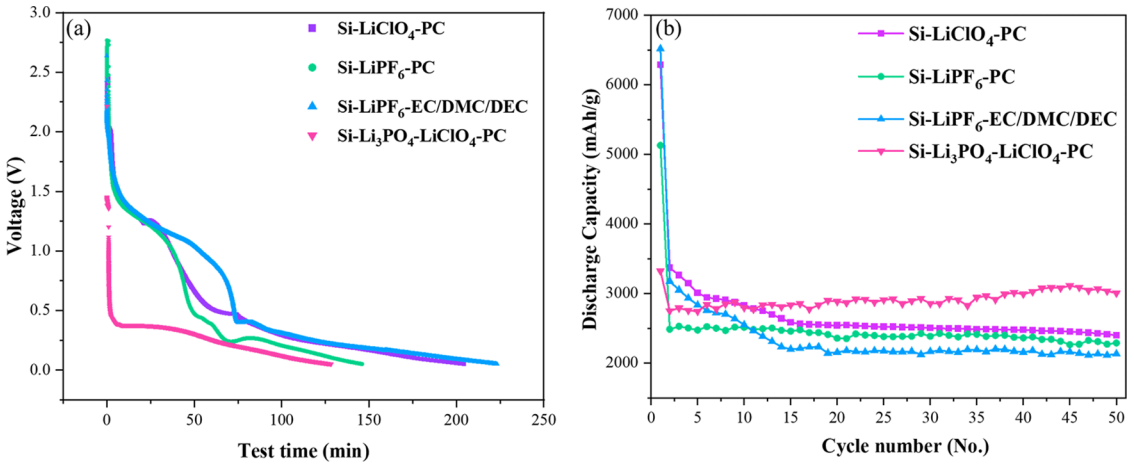

Figure 1. Electrochemical measurements of Si electrodes in different liquid electrolytes. (a) First discharge curves of Si and Si-Li_3PO_4 anodes in $LiClO_4$-based and $LiPF_6$-based electrolytes. (b) Discharge capacities of Si and Si-Li_3PO_4 anodes in different electrolytes.

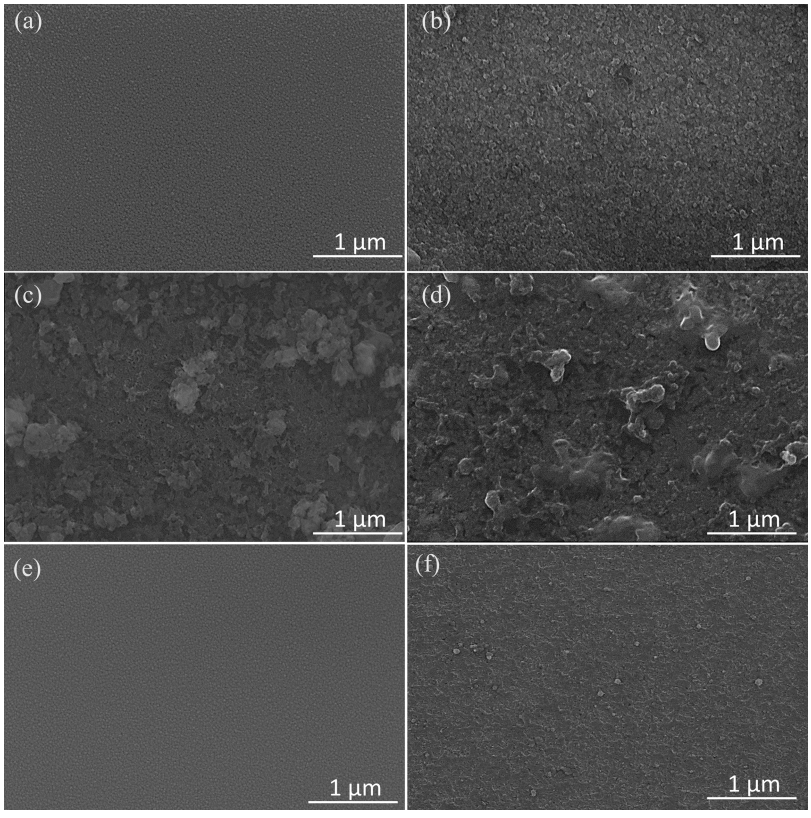

Figure 2. SEM image of the pristine Si thin film (a) and after cycling with $LiClO_4$ in PC solvents (b), $LiPF_6$ in PC solvents (c), and $LiPF_6$ in EC/EDC/DMC solvents (d). SEM image of the pristine Si-Li_3PO_4 thin film (e) and after cycling with $LiClO_4$ in PC solvents (f).

where $\alpha = (A_1, A_2, A_3)'$, $y = (\log([a_0 - V_1]^2), ..., \log([a_0 - V_N]^2))'$, $\varepsilon = (\varepsilon_1,...,\varepsilon_N)'$, and matrix X is defined as

$$X = \begin{pmatrix} 1 & \log(t_1) & \log(\log(t_1)) \\ 1 & \log(t_2) & \log(\log(t_2)) \\ \vdots & \vdots & \vdots \\ 1 & \log(t_N) & \log(\log(t_N)) \end{pmatrix} \quad (5)$$

First, the initial guess of a_0 can be obtained, for example, by adding 100 mV to the last observed voltage sample. After that, the initial OLS estimator is obtained for α, *i.e.*, $\hat{\alpha} = (\hat{A}_1, \hat{A}_2, \hat{A}_3)'$, where $\hat{\alpha} = (X' X)^{-1} X' y$. Then, the squared sum error $\|y - X\hat{\alpha}\|^2$ is calculated. This procedure is repeated for a number of initial guesses from the interval around a_0. The size of the interval and the number of points are adjustable parameters of the method. The point where the minimal value for $\|y - X\hat{\alpha}\|^2$ is achieved is taken as $\hat{\alpha}_0$. This approach leads to a more straightforward implementation than numerical minimizing $\|y - X\hat{\alpha}\|^2$ with respect to a_0 and α jointly. Finally, the parameters in the original model of eq 1 will be recovered as $\hat{\alpha}_1 = -\hat{A}_2/2$, $\hat{\alpha}_2 = -\hat{A}_3/2$, and $\hat{\alpha}_3 = \exp(\hat{A}_1/2)$. Since there are four unknown parameters a_i (for i from 0 to 3) in eq 1, at least four sample points are needed to solve the set of equations, i.e., $N \geq 4$.

https://doi.org/10.1021/acsomega.2c04415
ACS Omega 2022, 7, 32740−32748

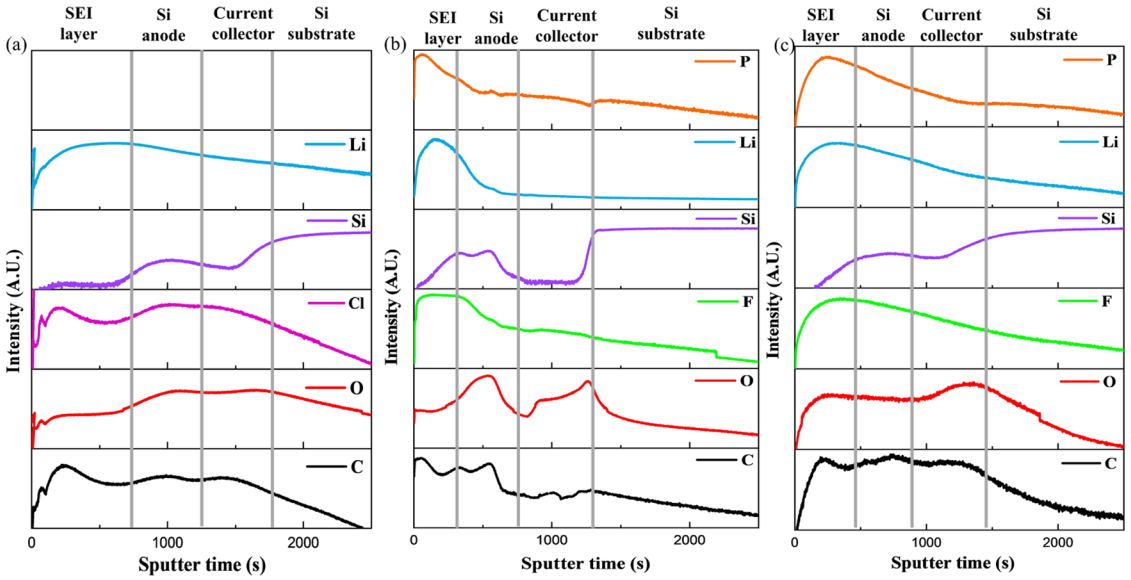

Figure 3. Sputter-etched TOF-SIMS spectra of Si electrodes after GITT measurements in $LiClO_4$-based electrolytes (a), $LiPF_6$ in PC solvents (b), and $LiPF_6$ in EC/EDC/DMC solvents (c).

3. RESULTS AND DISCUSSION

Amorphous Si thin films (50 nm) deposited by PVD were electrochemically characterized in $LiClO_4$-based and $LiPF_6$-based electrolytes. The first discharge cycle profiles of Si-based anodes in different electrolytes and corresponding differential discharge capacity profiles are shown in Figure 1. In Figure 1a, a short voltage plateau appears around 1 V, which is thought to be caused by the SEI formation through the decomposition of carbonaceous solvents and lithium salts.[38] However, the plateau duration differs in these samples, indicating that the formed SEI on the Si anode with $LiPF_6$ in EC/EDC/DMC solvents is thicker than in the other two samples. When using PC solvents, the SEI on the Si anode with $LiClO_4$ is slightly more than that of $LiPF_6$-based electrolytes. This observation indicates that both Li-salts and organic solvents will influence the SEI formation. The first discharge capacities of these samples are 6285, 5129, and 6517 mAh/g (as shown in Figure 1b), which also suggests different SEI formation mass/thickness. After 50 cycles, the discharge capacity of the three samples had already reached a relatively stable state. However, the stable capacity of the Si anode with $LiClO_4$-based electrolytes is higher, which indicates that the Si anode with $LiClO_4$-based electrolytes in PC performs higher reversible capacity and better stability. To further explore whether the SEI layer affects the stability of the Si electrode, an artificial layer of LPO was deposited on the Si surface. The same measurements were performed (as shown in Figure 1a,b), which will be discussed in detail in the subsequent sections.

To explore the SEI influence on the electrochemical stability of Si, we compared the SEI morphology and composition with different electrolytes. SEM images of fresh Si thin films and cycled Si anodes with different electrolytes are shown in Figure 2. Compared with the as-deposited Si films (Figure 2a), the cycled Si shows a relatively rough surface morphology (Figure 2b–d). Notably, the surfaces of Si cycled with $LiPF_6$ in PC or EC/DMC/DEC solvents (Figure 2c,d) are rougher than with $LiClO_4$-based electrolytes (Figure 2b). It seems denser and smoother, which is beneficial for Li^+ transport in Si electrodes.

To check the SEI composition, sputter-etched ToF-SIMS analyses were performed for the Si electrodes cycled with different electrolytes. Figure 3a–c shows the C, O, Li, Cl (F), Si, Li, and P spectra of the Si samples (rinsed by PC or DMC and dried) after the discharging process. Four zones are observed based on Si spectra with corresponding zones marked by vertical gray lines: SEI layer (before the Si area), Si thin-film electrode, current collector, and Si substrate. As shown in Figure 3a, the first peak of the Si element in the Si anode with $LiClO_4$-based electrolytes appeared near the sputtering time of 1000 s, which indicates that the sputtering time ranging from 0 to 750 s corresponds to the SEI layer. In the SEI layer, there are two peaks of chlorine. One is in the outermost layer of the SEI layer. The other is in the place closest to the Si film but less in the middle, which indicates that LiCl is distributed in the outermost and innermost layers of the SEI layer.[39] Carbon is primarily distributed in the outer SEI layer. In the inner part near the Si film, the carbon content is low, indicating that organic species, such as $ROCO_2Li$ (where R is a low-molecular-weight alkyl group), are mainly distributed in the outer SEI layer. The content of O and Li in the inner layer is high, indicating that the inner SEI layer is primarily composed of inorganic oxygenates, such as Li_2O and Li_2CO_3.[39] However, Figure 3b,c shows that the F and carbon contents are relatively high in the whole SEI layers, indicating that LiF and organic species are distributed homogeneously across the whole SEI layer formed in $LiPF_6$-based electrolytes.[40] The distribution of other elements in these samples is similar. Therefore, the difference in the composition of SEI layers formed in different electrolytes is LiCl and LiF. LiCl (Figure 3a) is only distributed in the outermost and innermost layers of the SEI layer. At the same time, LiF (Figure 3b,c) exists in the whole SEI layer, which may roughen the SEI layers. In addition, the electronegativity of fluorine is stronger than that of chlorine, which leads to a higher bond energy of Li–F (577 kJ/mol) than that of Li–Cl (469 kJ/mol) and other SEI compositions,[41] resulting in that LiF exhibits lower Li-ion diffusivity. Therefore, the SEI layer formed on the Si anode surface in $LiClO_4$-based electrolytes will be more beneficial for Li-ion diffusion than that formed in $LiPF_6$-based electrolytes.

A good SEI layer can prevent further electrolyte decomposition and stop the peeling of anode materials. However, the properties of the formed SEI layer, such as morphology and

https://doi.org/10.1021/acsomega.2c04415
ACS Omega 2022, 7, 32740–32748

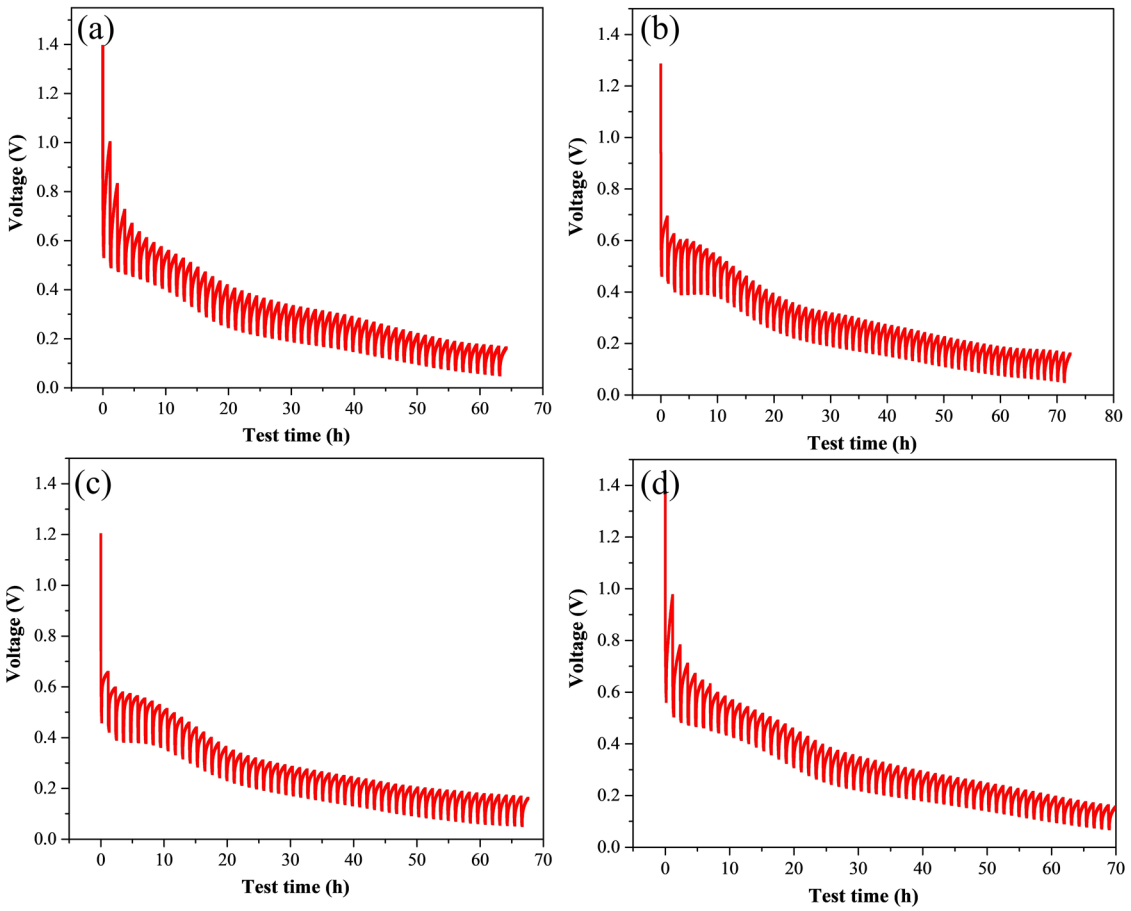

Figure 4. GITT measurement results of the Si anode with $LiClO_4$ in PC solvents (a), $LiPF_6$ in PC solvents (b), $LiPF_6$ in EC/EDC/DMC solvents (c), and the Si-Li_3PO_4 anode with $LiClO_4$ in PC solvents (d).

composition, highly depend on the electrolyte salts and organic solvents. Constructing an appropriate artificial layer on electrodes that suppresses the SEI formation could significantly improve the cycling stability of Si. For this purpose, a 60 nm Li_3PO_4 thin film was deposited on the Si surface (Figure 2e). The $LiClO_4$-based electrolytes were found to be more favorable for stability and continued to be used for testing. Figure 1a (pink line) shows the voltage drop of a Li_3PO_4-protected Si electrode in the first lithiation process. No SEI formation voltage plateau, at around 1 V, was observed, indicating that Li_3PO_4 can suppress the SEI formation. Due to the absence of SEI formation, the first discharge capacity of Li_3PO_4-protected Si (3323 mAh/g) is much lower than that of the pure Si thin film (Figure 1b). However, the second discharge capacity is near to the intimal capacity, and capacity retention (84.8%) is significantly higher than that of pure Si electrodes (56.1%) during the second cycle (Figure 1b). Compared with pure Si electrodes, the surface of the Si-Li_3PO_4 electrode is smoother after cycling (Figure 2e,f). This observation implies that Li_3PO_4 can suppress the SEI formation on Si anodes and serves as a protective layer to improve the capacity retention by reducing the chemical reaction between Si anodes and electrolytes.

The Li-ion diffusion coefficient is an essential parameter to evaluate the capability of an electrode for high-rate charging and discharging. Li-ions are easier to migrate and diffuse in electrode materials with a higher diffusion coefficient. GITT measurements were applied to evaluate the Li-ion diffusion coefficient (D_{Li^+}) in Si electrodes. In the GITT experiments, the working electrodes were initially loaded with a constant current pulse (0.15 C) at t_0, and this pulse was held for 10 min. Subsequently, the current was disconnected and rested for 1 h. The voltage between the working electrode and the reference electrode was measured until an equilibrium value V_s was achieved. Figure 4 shows the GITT voltage curves as a function of test time for the Si electrodes.

The potential change during a single pulse and subsequent relaxation in GITT measurement with $LiClO_4$ in PC electrolytes is illustrated in Figure 5a. Compared with the GITT results from other literature with a relaxation time of 20 min,[29,31] the relaxation time used here is longer. However, the potential does not reach a complete equilibrium state even at the end of the relaxation period, with a slight increase occurring throughout the relaxation period. A possible reason could be the side reactions that occur during the relaxation period.[31] To minimize these effects, a voltage-relaxation model[37] was applied to predict the relaxation voltage during a 3 h relaxation time (Figure 5a). As shown in Figure 6a–d, the measured voltage curves (blue line) still have an upward trend with a relaxation time of 1 h. However, the predicted relaxation voltages (pink line) at a relaxation time of 3 h are far closer to equilibrium.

Moreover, it was discovered that skipping the starting part of the relaxation period improves fit and prediction. The parts of the relaxation voltages that have been skipped are marked by green dots. Based on the predicted voltages, the EMF curves are shown in Figure 5b–e. It was found that a plateau when the voltage is near 0.5–0.6 V in the pure Si anodes is due to the

https://doi.org/10.1021/acsomega.2c04415
ACS Omega 2022, 7, 32740–32748

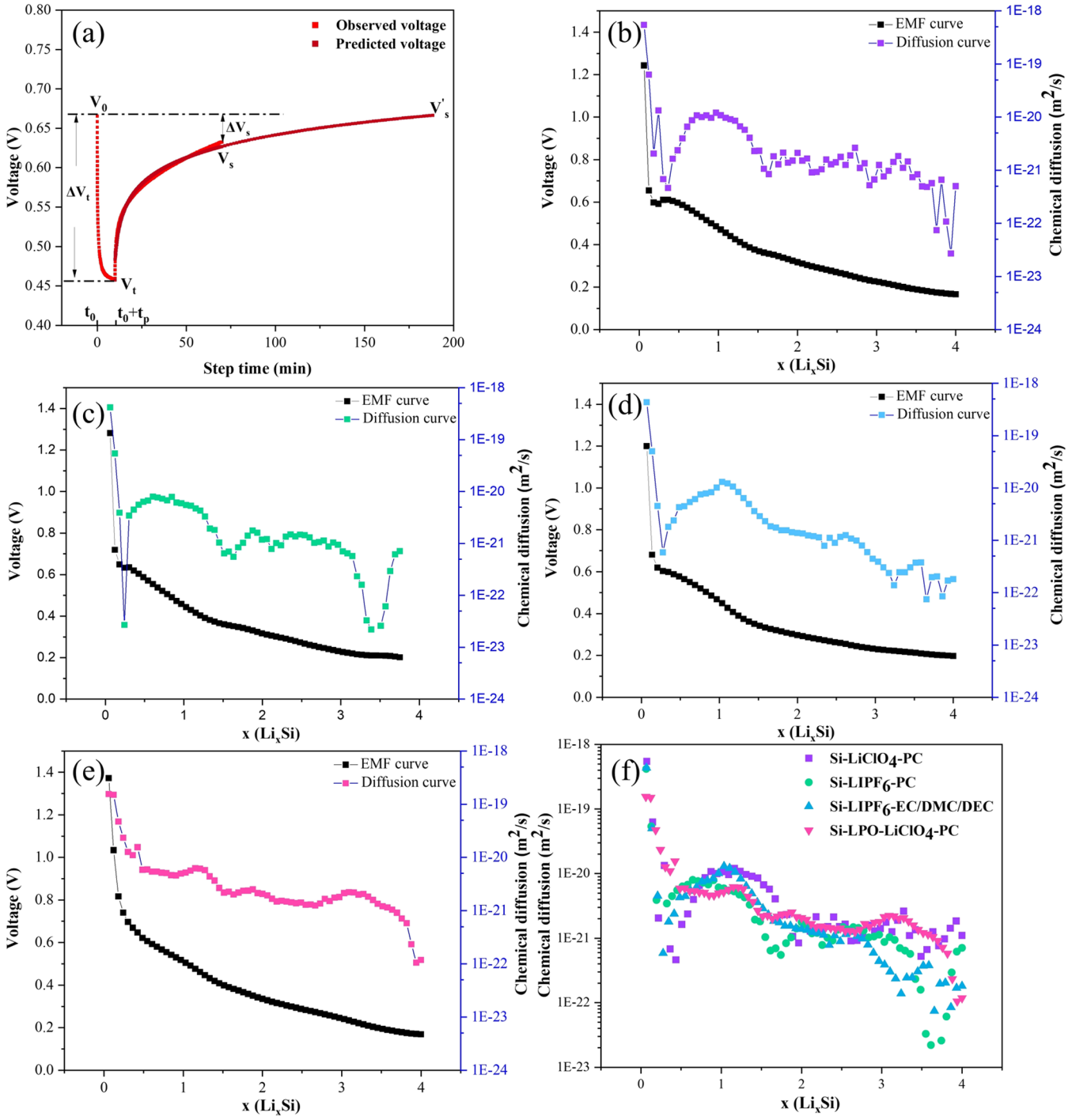

Figure 5. EMF and Li diffusion coefficient curves. (a) Characteristic pulse of observed voltages and predicted voltages in an enlarged view in GITT measurement with $LiClO_4$ in PC electrolytes; (b) EMF curve and chemical diffusivities of Li from GITT measurements for the Si anode with $LiClO_4$ in PC electrolytes; (c) EMF curve and chemical diffusivities of Li from GITT measurements for the Si anode with $LiPF_6$ in PC solvents; (d) EMF curve and chemical diffusivities of Li from GITT measurements for the Si anode with $LiPF_6$ in EC/EDC/DMC solvents; (e) EMF curve and chemical diffusivities of Li from GITT measurements for the Si-Li_3PO_4 anode with $LiClO_4$ in PC electrolytes; and (f) chemical diffusion curves of Li for Si and Si-Li_3PO_4 anodes in $LiClO_4$-based and $LiPF_6$-based electrolytes.

formation of SEI layers. However, the whole plateau becomes almost invisible in the Li_3PO_4-protected Si anode, confirming that Li_3PO_4 can suppress the SEI formation.

Further, the effect of the SEI layer on the estimated Li-ion diffusion coefficients is discussed. The diffusion coefficients (D_{Li^+}) of Li-ions were calculated according to eq 6, derived from Fick's second law[42]

$$D_{Li^+} = \frac{4}{\pi t_p}\left(\frac{m_B V_M}{M_B S}\right)^2\left(\frac{\Delta V_s}{\Delta V_t}\right)^2 \quad (\tau'' L^2/D_{Li^+}) \tag{6}$$

Here, where m_B is the weight of the electrode material, V_M [cm^3/mol] is the molar volume, M_B [g/mol] is the molar weight, S [cm^2] is the area of the electrode−electrolyte interface, L [cm] is the electrode thickness, ΔV_t is the measured potential change

https://doi.org/10.1021/acsomega.2c04415
ACS Omega 2022, 7, 32740−32748

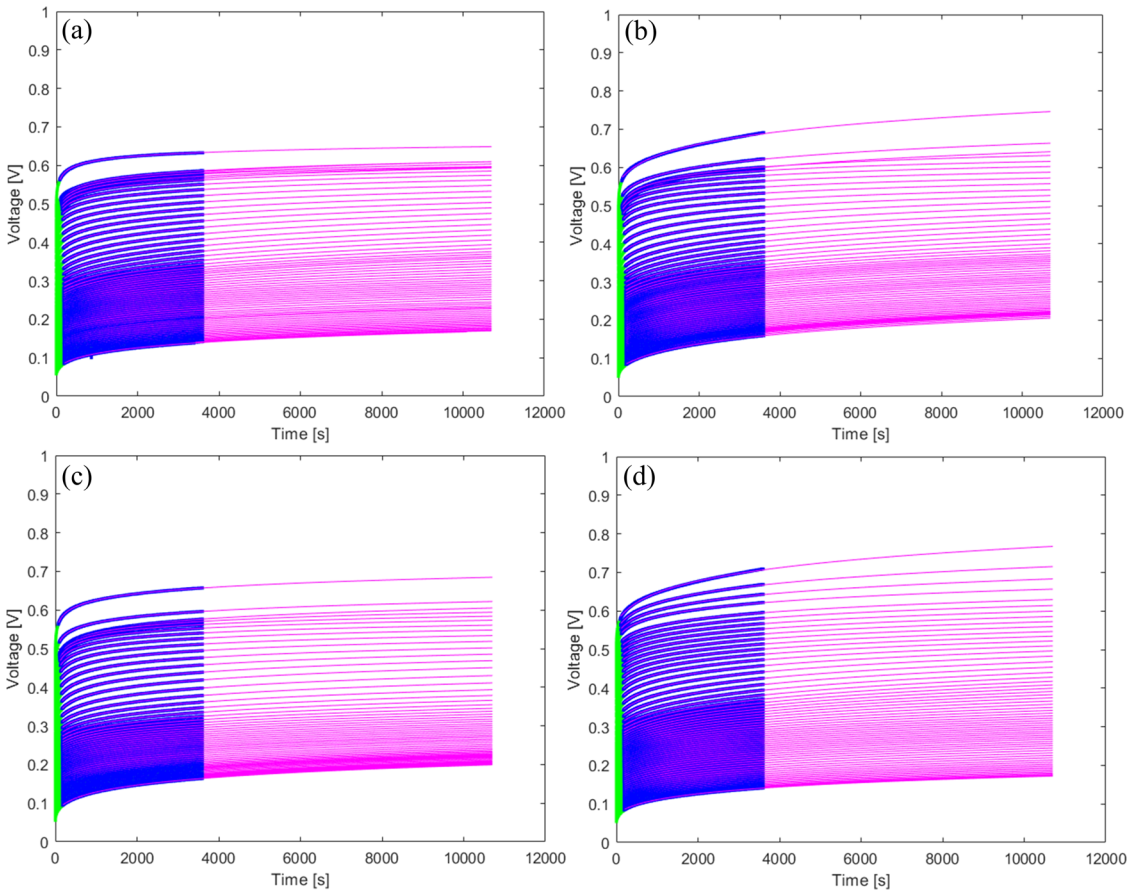

Figure 6. Measured voltage curves (blue) and predicted voltage curves (pink) as a function of the relaxation time for Si anodes with $LiClO_4$ in PC electrolytes (a); Si anode with $LiPF_6$ in PC solvents (b); Si anode with $LiPF_6$ in EC/EDC/DMC solvents (c); and Si-Li_3PO_4 anode with $LiClO_4$ in PC electrolytes (d).

during the current pulse, and ΔV_S is the difference in the potential at the end of two subsequent relaxation periods (Figure 5a). Since the working electrode is assumed to be in equilibrium at the end of the relaxation period, the predicted voltage is more suitable for calculating the Li-ion diffusion coefficients.

The Li-ion diffusion coefficients D_{Li^+} calculated using eq 6 and predicted equilibrium voltages are plotted in Figure 5b−e as a function of the stoichiometric index x (in Li_xSi). In these curves, there are similar values and similar "W" shapes. This phenomenon is consistent with the findings of earlier studies.[29,31] Because Li^+ diffusion could take place through the phase border and inside each phase while being strongly accompanied by interactions with other nearby ions, there was a significant shift in the chemical diffusion coefficient of Li^+ in the two-phase area. Therefore, the calculated D_{Li+} is just an apparent value.[43] Here, Si anodes in $LiClO_4$-based electrolytes are represented to be discussed. The results are shown in Figure 5b, where the (estimated) equilibrium voltages and chemical diffusivities are plotted as a function of relative Li concentration x. The Li-ion diffusion coefficient curves exhibit a shape similar to the letter "W", consistent with earlier published results.[31] For the first pulse, the diffusivity is observed to start at $\sim 5 \times 10^{-19}$ m^2/s. It subsequently decreases by 3 orders of magnitude to a minimum of 1×10^{-22} m^2/s near $x \approx 0.5$. Afterward, the diffusivity increases again to around 1×10^{-21} m^2/s at $x \approx 1$, where a local maximum is reached.

In general, diffusivity drops with lithiation. However, there are local humps aligned with slopes and plateaus on the voltage curve. When comparing the calculated Li-ion diffusion coefficients of the various samples with an experiment relaxation time of 1 h (Figure S2) and extended time of 3 h (Figure 5f), the estimated values of the lithium-ion diffusion coefficients for the voltage-prediction method have the same order of magnitude as values based on experimentally measured voltages. However, there is less noise visible, and there is less difference between various samples. That indicates that the lithium-ion diffusion coefficients estimated on the base of the voltage-prediction method are more accurate. In addition, it turns out that the values of chemical diffusivities are similar. The protective layer, therefore, does not improve the Li-ion diffusivity of Si electrodes. The fact that all diffusion coefficients are similar can be attributed to the rate-determining property of the diffusion rate in the Si electrodes. Since the Si layers are all of the same, the diffusion process must be similar in all electrodes. Therefore, the observed spread between the curves in Figure 5f can be attributed to the measurement and/or simulation error.

4. CONCLUSIONS

SEI formation at the electrode/electrolyte interface significantly influences the cycling stability of Si anodes. Herein, we found that Si anodes with $LiClO_4$-based electrolytes are more stable than those with $LiPF_6$-based electrolytes. This observation is attributed to the fact that the SEI on Si formed with $LiClO_4$-based electrolytes is dense, hard, relatively homogeneous, and

https://doi.org/10.1021/acsomega.2c04415
ACS Omega 2022, 7, 32740−32748

with a main component of LiCl. In the case of using $LiPF_6$-based electrolytes, LiF is the main phase in SEI. Si has a better cycling performance in $LiClO_4$-based electrolytes than in $LiPF_6$-based electrolytes, which can be explained by the fact that LiCl has better Li-ionic conductivity than LiF. In addition, Li_3PO_4 was deposited on the Si surface to suppress the SEI layer formation and improve the coulombic efficiency and stability. Finally, GITT measurements were carried out on the various Si electrodes. The relaxation times were extended to 3 h by the voltage-prediction method to reach a state closer to the equilibrium. The corresponding Li-ion diffusion coefficients calculated during the discharge process range from 10^{-23} to 10^{-19} cm^2/s.

■ ASSOCIATED CONTENT

Supporting Information

The Supporting Information is available free of charge at https://pubs.acs.org/doi/10.1021/acsomega.2c04415.

Profilometer measurements of Li_3PO_4 film thickness and chemical diffusion curves of Li for Si anodes in $LiClO_4$-based and $LiPF_6$-based electrolytes calculated by experimental voltages with a relaxation time of 1 h (PDF)

■ AUTHOR INFORMATION

Corresponding Authors

Chunguang Chen − *Forschungszentrum Jülich (IEK-9), D-52425 Jülich, Germany; LNM, Institute of Mechanics, Chinese Academy of Sciences, Beijing 100190, China*; Email: chenchunguang@imech.ac.cn

Peter H. L. Notten − *Forschungszentrum Jülich (IEK-9), D-52425 Jülich, Germany; Eindhoven University of Technology, 5600 MB Eindhoven, The Netherlands; University of Technology Sydney, Sydney, NSW 2007, Australia*; orcid.org/0000-0003-4907-8426; Email: p.h.l.notten@tue.nl

Authors

Baolin Wu − *Forschungszentrum Jülich (IEK-9), D-52425 Jülich, Germany; RWTH Aachen University, D-52074 Aachen, Germany*

Dmitri L. Danilov − *Forschungszentrum Jülich (IEK-9), D-52425 Jülich, Germany; Eindhoven University of Technology, 5600 MB Eindhoven, The Netherlands*

Ming Jiang − *Forschungszentrum Jülich (IEK-9), D-52425 Jülich, Germany; Eindhoven University of Technology, 5600 MB Eindhoven, The Netherlands*

Luc H. J. Raijmakers − *Forschungszentrum Jülich (IEK-9), D-52425 Jülich, Germany*

Rüdiger-A. Eichel − *Forschungszentrum Jülich (IEK-9), D-52425 Jülich, Germany; RWTH Aachen University, D-52074 Aachen, Germany*; orcid.org/0000-0002-0013-6325

Complete contact information is available at: https://pubs.acs.org/10.1021/acsomega.2c04415

Author Contributions

The manuscript was written with the contributions of all authors. All authors have approved the final version of the manuscript.

Notes

The authors declare no competing financial interest.

■ ACKNOWLEDGMENTS

B.W. gratefully acknowledges fellowship support from the China Scholarship Council. The authors thank ZEA-3 of Forschungszentrum Jülich for performing the ToF-SIMS measurements.

■ REFERENCES

(1) Chan, C. K.; Peng, H.; Liu, G.; McIlwrath, K.; Zhang, X. F.; Huggins, R. A.; Cui, Y. High-performance lithium battery anodes using silicon nanowires. *Nat. Nanotechnol.* **2008**, *3*, 31−35.

(2) Notten, P. H. L.; Roozeboom, F.; Niessen, R. A. H.; Baggetto, L. 3-D Integrated All-Solid-State Rechargeable Batteries. *Adv. Mater.* **2007**, *19*, 4564−4567.

(3) Jiménez, A. R.; Klöpsch, R.; Wagner, R.; Rodehorst, U. C.; Kolek, M.; Nölle, R.; Winter, M.; Placke, T. A Step toward High-Energy Silicon-Based Thin Film Lithium Ion Batteries. *ACS Nano* **2017**, *11*, 4731−4744.

(4) Mukanova, A.; Jetybayeva, A.; Myung, S.-T.; Kim, S.-S.; Bakenov, Z. A mini-review on the development of Si-based thin film anodes for Li-ion batteries. *Mater. Today Energy* **2018**, *9*, 49−66.

(5) Galvez-Aranda, D. E.; Verma, A.; Hankins, K.; Seminario, J. M.; Mukherjee, P. P.; Balbuena, P. B. Chemical and mechanical degradation and mitigation strategies for Si anodes. *J. Power Sources* **2019**, *419*, 208−218.

(6) Zhang, W.-J. A review of the electrochemical performance of alloy anodes for lithium-ion batteries. *J. Power Sources* **2011**, *196*, 13−24.

(7) Meister, P.; Jia, H.; Li, J.; Kloepsch, R.; Winter, M.; Placke, T. Best Practice: Performance and Cost Evaluation of Lithium Ion Battery Active Materials with Special Emphasis on Energy Efficiency. *Chem. Mater.* **2016**, *28*, 7203−7217.

(8) Baggetto, L.; Niessen, R. A. H.; Notten, P. H. L. On the activation and charge transfer kinetics of evaporated silicon electrode/electrolyte interfaces. *Electrochim. Acta* **2009**, *54*, 5937−5941.

(9) McDowell, M. T.; Lee, S. W.; Nix, W. D.; Cui, Y. 25th Anniversary Article: Understanding the Lithiation of Silicon and Other Alloying Anodes for Lithium-Ion Batteries. *Adv. Mater.* **2013**, *25*, 4966−4985.

(10) Uxa, D.; Jerliu, B.; Hüger, E.; Dörrer, L.; Horisberger, M.; Stahn, J.; Schmidt, H. On the Lithiation Mechanism of Amorphous Silicon Electrodes in Li-Ion Batteries. *J. Phys. Chem. C* **2019**, *123*, 22027−22039.

(11) Peled, E.; Yamin, H. Solid Electrolyte Interphase (SEI) Electrodes. Part 1. The Kinetics of Lithium in $LiAlCl_4$-$SOCl_2$. *Isr. J. Chem.* **1979**, *18*, 131−135.

(12) Trill, J.-H.; Tao, C.; Winter, M.; Passerini, S.; Eckert, H. NMR investigations on the lithiation and delithiation of nanosilicon-based anodes for Li-ion batteries. *J. Solid State Electrochem.* **2011**, *15*, 349−356.

(13) Zhang, Y.; Du, N.; Yang, D. Designing superior solid electrolyte interfaces on silicon anodes for high-performance lithium-ion batteries. *Nanoscale* **2019**, *11*, 19086−19104.

(14) Zheng, J.; Zheng, H.; Wang, R.; Ben, L.; Lu, W.; Chen, L.; Chen, L.; Li, H. 3D visualization of inhomogeneous multi-layered structure and Young's modulus of the solid electrolyte interphase (SEI) on silicon anodes for lithium ion batteries. *Phys. Chem. Chem. Phys.* **2014**, *16*, 13229−13238.

(15) Wang, A.; Kadam, S.; Li, H.; Shi, S.; Qi, Y. Review on modeling of the anode solid electrolyte interphase (SEI) for lithium-ion batteries. *npj Comput. Mater.* **2018**, *4*, 15.

(16) Benitez, L.; Cristancho, D.; Seminario, J. M.; Martinez de la Hoz, J. M.; Balbuena, P. B. Electron transfer through solid-electrolyte-interphase layers formed on Si anodes of Li-ion batteries. *Electrochim. Acta* **2014**, *140*, 250−257.

(17) Soto, F. A.; Ma, Y.; Martinez de la Hoz, J. M.; Seminario, J. M.; Balbuena, P. B. Formation and Growth Mechanisms of Solid-Electrolyte Interphase Layers in Rechargeable Batteries. *Chem. Mater.* **2015**, *27*, 7990−8000.

(18) Verma, P.; Maire, P.; Novák, P. A review of the features and analyses of the solid electrolyte interphase in Li-ion batteries. *Electrochim. Acta* **2010**, *55*, 6332−6341.

(19) Yang, L.; Cheng, X.; Ma, Y.; Lou, S.; Cui, Y.; Guan, T.; Yin, G. Changing of SEI Film and Electrochemical Properties about MCMB Electrodes during Long-Term Charge/Discharge Cycles. *J. Electrochem. Soc.* **2013**, *160*, A2093−A2099.
(20) Guan, P.; Liu, L.; Lin, X. Simulation and Experiment on Solid Electrolyte Interphase (SEI) Morphology Evolution and Lithium-Ion Diffusion. *J. Electrochem. Soc.* **2015**, *162*, A1798−A1808.
(21) Xia, H.; Tang, S.; Lu, L. Properties of amorphous Si thin film anodes prepared by pulsed laser deposition. *Mater. Res. Bull.* **2007**, *42*, 1301−1309.
(22) Kulova, T. L.; Skundin, A. M.; Pleskov, Y. V.; Terukov, E. I.; Kon'kov, O. I. Lithium intercalation in thin amorphous-silicon films. *Russ. J. Electrochem.* **2006**, *42*, 363−369.
(23) Kulova, T. L.; Skundin, A. M.; Pleskov, Y. V.; Terukov, E. I.; Kon'kov, O. I. Lithium insertion into amorphous silicon thin-film electrodes. *J. Electroanal. Chem.* **2007**, *600*, 217−225.
(24) Kulova, T. L.; Pleskov, Y. V.; Skundin, A. M.; Terukov, E. I.; Kon'kov, O. I. Lithium intercalation into amorphous-silicon thin films: An electrochemical-impedance study. *Russ. J. Electrochem.* **2006**, *42*, 708−714.
(25) Zhang, T.; Zhang, H. P.; Yang, L. C.; Wang, B.; Wu, Y. P.; Takamura, T. The structural evolution and lithiation behavior of vacuum-deposited Si film with high reversible capacity. *Electrochim. Acta* **2008**, *53*, 5660−5664.
(26) Li, J.; Xiao, X.; Yang, F.; Verbrugge, M. W.; Cheng, Y.-T. Potentiostatic Intermittent Titration Technique for Electrodes Governed by Diffusion and Interfacial Reaction. *J. Phys. Chem. C* **2012**, *116*, 1472−1478.
(27) Yoshimura, K.; Suzuki, J.; Sekine, K.; Takamura, T. Evaluation of the Li insertion/extraction reaction rate at a vacuum-deposited silicon film anode. *J. Power Sources* **2005**, *146*, 445−447.
(28) Xie, J.; Imanishi, N.; Zhang, T.; Hirano, A.; Takeda, Y.; Yamamoto, O. Li-ion diffusion in amorphous Si films prepared by RF magnetron sputtering: A comparison of using liquid and polymer electrolytes. *Mater. Chem. Phys.* **2010**, *120*, 421−425.
(29) Ding, N.; Xu, J.; Yao, Y. X.; Wegner, G.; Fang, X.; Chen, C. H.; Lieberwirth, I. Determination of the diffusion coefficient of lithium ions in nano-Si. *Solid State Ionics* **2009**, *180*, 222−225.
(30) Nguyen, S. H.; Lim, J. C.; Lee, J. K. Electrochemical characteristics of bundle-type silicon nanorods as an anode material for lithium ion batteries. *Electrochim. Acta* **2012**, *74*, 53−58.
(31) Uxa, D.; Hüger, E.; Schmidt, H. Li Diffusion in Thin-Film LiySi Electrodes: Galvanostatic Intermittent Titration Technique and Tracer Diffusion Experiments. *J. Phys. Chem. C* **2020**, *124*, 27894−27899.
(32) Horner, J. S.; Whang, G.; Ashby, D. S.; Kolesnichenko, I. V.; Lambert, T. N.; Dunn, B. S.; Talin, A. A.; Roberts, S. A. Electrochemical Modeling of GITT Measurements for Improved Solid-State Diffusion Coefficient Evaluation. *ACS Appl. Energy Mater.* **2021**, *4*, 11460−11469.
(33) Pop, V.; Bergveld, H. J.; Danilov, D.; Regtien, P.; Notten, P. *Battery Management Systems: Accurate State-of-Charge Indication for Battery-Powered Applications*, Springer Publishing Company Incorporated, 2008.
(34) Jiang, M.; Wu, X.; Zhang, Q.; Danilov, D. L.; Eichel, R.-A.; Notten, P. H. L. Fabrication and interfacial characterization of Ni-rich thin-film cathodes for stable Li-ion batteries. *Electrochim. Acta* **2021**, *398*, No. 139316.
(35) Aylor, J. H.; Thieme, A.; Johnso, B. W. A battery state-of-charge indicator for electric wheelchairs. *IEEE Trans. Ind. Electron.* **1992**, *39*, 398−409.
(36) Hoening, S.; Singh, H.; Palanisamy, T. G.Method for Determining State of Charge of a Battery by Measuring Its Open Circuit Voltage. US Patent US6366054B1, 2002.
(37) Bergveld, H. J.; Pop, V.; Notten, P. H. L. Apparatus and Method for Determining of the State-of-Charge of a Battery When the Battery is NOT in Equilibrium. European Patent EP2089731, 2010.
(38) Xu, K. Nonaqueous Liquid Electrolytes for Lithium-Based Rechargeable Batteries. *Chem. Rev.* **2004**, *104*, 4303−4418.
(39) Pereira-Nabais, C.; Światowska, J.; Rosso, M.; Ozanam, F.; Seyeux, A.; Gohier, A.; Tran-Van, P.; Cassir, M.; Marcus, P. Effect of Lithiation Potential and Cycling on Chemical and Morphological Evolution of Si Thin Film Electrode Studied by ToF-SIMS. *ACS Appl. Mater. Interfaces* **2014**, *6*, 13023−13033.
(40) Chen, C.; Zhou, T.; Danilov, D. L.; Gao, L.; Benning, S.; Schön, N.; Tardif, S.; Simons, H.; Hausen, F.; Schülli, T. U.; Eichel, R. A.; Notten, P. H. L. Impact of dual-layer solid-electrolyte interphase inhomogeneities on early-stage defect formation in Si electrodes. *Nat. Commun.* **2020**, *11*, No. 3283.
(41) Schiffer, H.; Ahlrichs, R. The C-Li bond in methyllithium. Binding energy and ionic character. *Chem. Phys. Lett.* **1986**, *124*, 172−176.
(42) Weppner, W.; Huggins, R. A. Determination of the Kinetic Parameters of Mixed-Conducting Electrodes and Application to the System Li_3Sb. *J. Electrochem. Soc.* **1977**, *124*, 1569−1578.
(43) Wang, J.; Li, X.; Wang, Z.; Guo, H.; Huang, B.; Wang, Z.; Yan, G. Systematic investigation on determining chemical diffusion coefficients of lithium ion in $Li_{1+x}VPO_4F$ $(0 \leq x \leq 2)$. *J. Solid State Electrochem.* **2015**, *19*, 153−160.

https://doi.org/10.1021/acsomega.2c04415
ACS Omega 2022, 7, 32740−32748